

RSC Advances

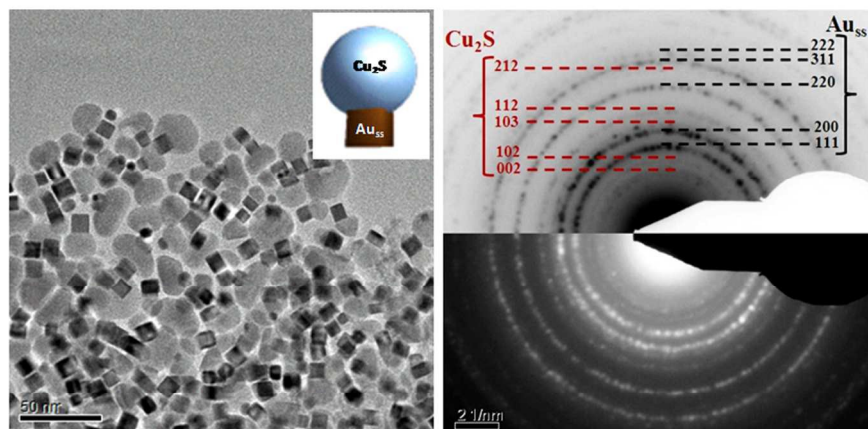


This is an *Accepted Manuscript*, which has been through the Royal Society of Chemistry peer review process and has been accepted for publication.

Accepted Manuscripts are published online shortly after acceptance, before technical editing, formatting and proof reading. Using this free service, authors can make their results available to the community, in citable form, before we publish the edited article. This *Accepted Manuscript* will be replaced by the edited, formatted and paginated article as soon as this is available.

You can find more information about *Accepted Manuscripts* in the [Information for Authors](#).

Please note that technical editing may introduce minor changes to the text and/or graphics, which may alter content. The journal's standard [Terms & Conditions](#) and the [Ethical guidelines](#) still apply. In no event shall the Royal Society of Chemistry be held responsible for any errors or omissions in this *Accepted Manuscript* or any consequences arising from the use of any information it contains.



Hybrid Nanoparticles Containing Solid Solution Au-Cu and Cu_2S phases

254x190mm (96 x 96 DPI)

Morphology Control Synthesis of Au-Cu₂S Metal-Semiconductor Hybrid Nanostructures by Modulating Reaction Constituents

S. K. Sinha^a, C. Srivastava^a, S. Sampath^b and K. Chattopadhyay^{a#}

^aDepartment of Materials Engineering, Indian Institute of Science, Bangalore-560 012, India,

^bDepartment of Inorganic and Physical Chemistry, Indian Institute of Science,

Bangalore-560 012, India

[#]corresponding author: Email: kamanio@materials.iisc.ernet.in

Phone: 91-080-22932262

FAX: 91-080-23600472

Abstract

A facile methodology for synthesizing Au–Cu₂S hybrid nanoparticles is presented. Au–Cu₂S nanoparticles have application in visible light driven photocatalytic degradation of dyes. Detailed microstructural and compositional characterization illustrated that the hybrid nanoparticles are composed of cube shaped Au–Cu solid solution and hemispherical shaped Cu₂S phases. Investigation of nanoparticles extracted at different stages of the synthesis process revealed that the mechanism of formation of hybrid nanoparticles involved initial formation of isolated cube shaped pure Au nanoparticles and Cu-thiolate complex. In the subsequent stages, the Au nanoparticles get adsorbed onto the Cu-thiolate complex which is followed by the decomposition of the Cu-thiolate complex to form Au–Cu₂S hybrid nanoparticles. This study also illustrates that an optimum concentration of dodecanethiol is required both for achieving size and morphological uniformity of the participating phases and for their attachment to form a hybrid nanoparticle.

Keywords: **Au-Cu₂S** hybrid nanoparticles, Electron microscopy, Morphology control, Chemical synthesis.

Introduction

Colloidal hybrid nanostructures¹⁻⁴ which are composed of two different solid-state phases sharing a heterophase interface have gained significance as multifunctional materials with applications in areas such as solar energy conversion and production,⁵⁻⁸ catalysis,⁹⁻¹¹ biological imaging¹², sensing¹³, electronics¹⁴, magnetism¹⁵, etc. These hybrid nanostructures exhibit physical and chemical properties that are distinctly different from the properties of the component phases and are derived essentially from the synergistic response of the component phases to a stimulus^{16,17}. Properties exhibited by hybrid nanoparticles can therefore be tuned by tailoring size, shape, composition and mutual orientation of the participating phases^{18,19}.

Synthesis methodology that is popularly adopted to produce hybrid nanostructures is seed mediated growth²⁰⁻²⁴. In this two-step process, pre-synthesized nano-solids of one of the phases serve as a heterogeneous site over which the other phase nucleates and grows to form the hybrid nanostructure. In this two step method, morphology and microstructure of the as-synthesized hybrid nanoparticles is mainly decided by the criterion of minimization of total surface energy which essentially is composed of the specific surface energies of the two participating phases and the heterophase interface between them. For a fixed volume of phases, a configuration that yields lowest surface energy value becomes stable. In the wet chemical synthesis technique for synthesizing nanoparticles, surface energies can be modified by the attachment of foreign species such as surfactants, ligands, etc to the nanoparticle surface²⁵. Therefore a precise control over the

type and amount of surfactants is required to tune the morphology and microstructure of the hybrid nanoparticles.

Hybrid nanoparticles containing Au and Cu₂S phases exhibit exploitable technological properties. These nanoparticles contained Au which is a well-known plasmonic metal and Cu₂S which is a p-type semiconductor known for its application in solar cell materials^{26,27}. It has been shown by Kim *et al*¹¹ that in Au-Cu₂S nanoparticles, transfer of electrons from Cu₂S to Au takes place. This transfer of electrons on one hand enhances the visible light driven oxidative degradation of dyes such as methylene blue and rhodamine B but on the other hand, suppresses the electrocatalytic activity of the Cu₂S phase towards the generation of H₂O₂ intermediaries which consequently decreases the degradation efficiency for 1,4-dioxane. Although there are few reports on the synthesis of Au-Cu₂S hybrid nanostructures²⁸⁻³⁰, tunable synthesis strategies that can control the size, morphology and orientation of the component phases is still lacking. The present study provides a synthesis strategy that produces uniform Au-Cu₂S hybrid nanoparticles. Here, uniformity implies particle-to-particle morphological and microstructural similarity. The study also investigates the formation mechanism of the hybrid nanoparticles by characterizing specimen extracted from the reaction mixture at different stages of the synthesis process.

Experiment

In the present study, modified polyol method was used for synthesizing Au-Cu₂S hybrid nanostructures^{31,32}. To synthesize Au-Cu₂S nanocrystals, 0.0339 g of tetrachloroauric acid [HAuCl₄], 0.0455 g of copper(II)acetylacetonate [Cu(acac)₂], 1.6 g of hexadecanediol (HDD), 2.0 g of hexadecylamine (HDA), 1.0 mL dodecanethiol (DDT) and 0.270 g 1-adamantanecarboxylic acid (ACA) were dissolved in 10 mL of diphenyl ether (DPE). This

reaction mixture was transferred to a three necks round bottom flask fitted with a reflux condenser and a magnetic stirrer. Temperature of the reaction mixture was increased gradually to $\sim 180^{\circ}\text{C}$ and was kept at this temperature for 5 hours. An inert atmosphere was maintained inside the three neck flask during the experiment. After 5 hours, heating was stopped and the reaction mixture was allowed to cool down to the room temperature. At the room temperature, the reaction mixture was poured into a beaker containing ethanol. Nanoparticles were isolated through high speed centrifugation and dispersed in hexane for further analysis.

X-Ray diffraction (XRD) technique was used for the identification of phases and average sizes of nanoparticles. XRD profiles were obtained from X-Pert PRO, PANalytical X-Ray diffractometer operating at 40 kV and 30 mA and using the Cu-K α radiation source. Specimens for the XRD based analysis were prepared by drop drying a dispersion of nanoparticles onto a glass slide. A FEI Tecnai F30 transmission electron microscope (TEM) operating at 300 keV was used for obtaining structural, compositional and morphological information both under normal transmission and scanning modes of operation. Samples for the TEM based analysis were prepared by drop drying a highly dilute dispersion of nanoparticles onto an electron transparent carbon coated Ni grid. Camera length used for obtaining the interplanar spacing values from the SAD patterns was calibrated using a polycrystalline Au standard. For three dimensional topographic imaging of nanoparticles in TEM, tilt angle in the range of -65° to $+65^{\circ}$ with a step size of 2° was used. Inspect 3D and Amira softwares were used for post alignment, reconstruction and visualization of the raw tomography data.

Results and Discussion

A representative bright field TEM image and STEM-HAADF image of as-synthesized Au-Cu₂S hybrid nanoparticles is shown in figure 1(a) and 1(b), respectively. These indicate that nanoparticles with a hemisphere-over-cube morphology have evolved after completion of the synthesis process. To illustrate the three-dimensional hemisphere-over-cube morphology of the as-synthesized hybrid nanoparticles, reconstructed images obtained from three-dimensional tomographic imaging of a representative hybrid nanoparticle in TEM is provided in figure 1(c). Other than these hybrid particles, no separate particles with only sphere, cube or any other morphology could be observed. Our results indicate that hemispherical phase has formed only on one face of the cubic phase, STEM-HAADF image shows a distinct difference in contrast between the cube and the hemispherical regions. As the image contrast in STEM-HAADF imaging is proportional to the atomic number, a difference in image contrast in figure 1(b) qualitatively indicates that the cube with bright contrast contains relatively more of the high atomic number component than the hemispherical region with relatively dull contrast. Average size (\pm standard deviation) of cube and hemispherical regions obtained from the analysis of several TEM bright field images are 9.0(\pm 1.5) nm and 18.0(\pm 4.7) nm respectively.

X-ray diffraction profile obtained from as-synthesized nanoparticles is shown in figure 1(d). The insert in figure 1(d) which shows the XRD profile in the 2θ range of 45-70° specifically reveals the diffraction peaks corresponding to the Cu₂S phase. Following observation can be made from the XRD profiles in figure 1(d): (i) X-ray diffraction profiles do not contain diffraction signature corresponding to pure Cu or its oxide phases indicating an absence of these phases in the as-synthesized nanoparticles (ii) the XRD profile exhibits peaks corresponding to

the hexagonal Cu_2S phase, (iii) lattice parameter value determined from the interplanar spacing corresponding to the high intensity peaks in the XRD profile matched with the lattice parameter value of a fcc gold solid solution with composition Au-20 at% Cu estimated using the Vegard's law^{33,34}. The XRD profile therefore indicated that the as-synthesized hybrid nanoparticles contained only Au-Cu solid solution and Cu_2S phases. Presence of Cu_2S and Au-Cu solid solution phases was also confirmed from the analysis of SAD patterns obtained from the as-synthesized nanoparticles. A representative SAD pattern obtained from a large group of nanoparticles showing the diffraction signature corresponding to the Cu_2S and Au-Cu solid solution is shown in figure 1(e). Relatively low intensity of the diffraction signals corresponding to the Cu_2S phase when compared to the diffraction signals corresponding to the Au-rich phase can be due to the large difference in the atomic scattering factors of the Au, Cu and S atoms and low symmetry of the Cu_2S phase when compared to the fcc Au-rich phase²⁹.

Compositional identity of the two phases within the nanoparticles was determined using the STEM-EDS analysis. Figure 2(a) shows the STEM-HAADF image of a representative two phase nanoparticles from which EDS signal was obtained. Compositional profile obtained from the region '2' in figure 2(a) revealed that the dull contrast hemispherical region contains 65 at% Cu and 35 at% S. Compositional profile obtained from the region marked '1' revealed that the bright contrast cube region contains 26 at% Cu and 74 at% Au. The atomic ratio of Cu-to-S in the hemispherical region was 1.86 ($\text{Cu/S} = 65/35$) which indicate a deficiency of Cu and formation of non-stoichiometric Cu_{2-x}S compound ($x=0.14$). STEM-EDS compositional mapping experiment was also performed to identify the spatial abundance of Au, Cu and S atoms within the hybrid nanoparticles. STEM-HAADF image of a representative nanoparticle, Au containing regions, Cu containing regions and S containing regions are shown in figure 2(b). It can be seen

from figure 2(b) that Au atoms are only present in the cube portion of the nanoparticle, whereas Cu and S atoms are distributed throughout the nanoparticle. The STEM-EDS compositional analysis results and the XRD data thus clearly illustrated that the hemispherical portion contains hexagonal Cu_2S phase and the cube portion contains Au-rich, Au–Cu solid solution phase.

Crystal structure of phases present in the cube and hemispherical regions was verified by the analysis of high resolution TEM (HRTEM) images of hybrid nanoparticles. HRTEM image of cube and spherical portions of a representative nanoparticle and the fast Fourier transform (FFT) pattern derived from the periodic lattice fringes in the HRTEM images are shown in figures 3(a-b). A single orientation of the lattice fringe in figures 3(a-b) indicates single crystalline nature of the cube and the hemisphere regions. The FFT pattern in inset of figure 3(a) matched perfectly with the diffraction pattern obtained from a standard fcc crystal oriented along [001] zone axis. The FFT pattern in figure 3(b) matched perfectly with the diffraction pattern obtained from a standard hcp crystal oriented along the [0001] zone axis. FFT patterns derived from the HRTEM images of the cube, sphere portion and cube-sphere interface regions of a representative hybrid nanoparticle are shown in figure 3(c). Magnified image of the interface in figure 3(c) clearly reveal that a diffuse interface boundary between cube and spherical phases which possibly is due to the diffusion of copper atoms into the gold across the interface. Recently, it has been reported using C_s -corrected STEM technique that diffusion of Cu atoms into Au region leads to rearrangement of lattice at the interface and formation of AuCu_3 ordered alloy phase at the surface³⁵. It is speculated that the diffusion of copper atoms into Au rich cube phase led to the formation of Au–Cu solid solution and copper deficient Cu_{2-x}S spherical phases. Additionally, It can be seen from the FFT patterns that the orientations of the cube and the

spherical phases is such that the [001] and [0001] directions and (200) and ($\bar{1}100$) planes in the fcc phase and hcp phase respectively are parallel to each other.

The mechanism of formation of $Au_{1-x}Cu_x-Cu_2S$ hybrid nanoparticle

In order to investigate the mechanism of formation of hybrid nanoparticles, reaction mixtures were extracted after 5, 180 and 300 minutes from the reaction solution maintained at 180°C. Nanoparticles present in the extracted reaction mixture are isolated by centrifugation for characterization.

XRD profiles obtained from samples extracted after 5, 180 and 300 minutes are shown in figure 4(a-d). Fig 4(a) contains XRD profiles for the full 2-theta range from 10 to 90; Fig 4(b) contains XRD profiles for the 2-theta range of 10 to 35; Fig 4(c) contains XRD profiles for the 2-theta range of 35 to 50; Fig 4(d) Contains XRD profiles for the 2-theta range of 50 to 90. Following observations can be made from the comparison of the XRD profiles in figure 4: (a) the highest intensity peak which corresponds to the (111) plane of the Au-rich fcc phase shifts to higher 2θ values with increase in the reaction time. This indicates Cu incorporation into the Au lattice with the progress of the synthesis process, (b) intensity of the diffraction peaks in the low 2θ value range (10° - $24^\circ 2\theta$ values) decreases with increase in the reaction time. These low angle (2θ) peaks were from the copper-thiolate complex as identified in the reference 31, (c) diffraction peaks corresponding to the hexagonal Cu_2S phase appears only in the diffraction profile obtained from the sample extracted after 300 min. The synergetic appearance and disappearance respectively of the diffraction peaks correspond to the Cu_2S and copper-thiolate complex and a shift in the fcc (111) peak indicates that during the initial stages of the synthesis process pure Au nanoparticles and Cu-thiolate complex form in the reaction mixture. With increase in time the

Cu-thiolate complex decomposes to form Cu atoms that are utilized in the formation of Cu_2S and solid solution of Au and Cu.

The mechanism proposed above for the formation of hybrid nanoparticle was supported by the results obtained through a TEM based analysis. TEM image of the sample extracted after 5 minutes revealed isolated cube shaped nanoparticles and cube shaped nanoparticles attached to a feature with a sheet like appearance as seen in figure 5(a-c). The sheet like feature in figure 5(c) is hence forth referred as “2D sheet”. Cube shaped nanoparticles were identified to be pure Au nanoparticles by STEM-EDS and electron diffraction based analysis. Figure 5(a) shows the TEM bright field image and the corresponding SAD pattern (in insert) of isolated cube shaped Au nanoparticles. Figure 5(b) shows TEM bright field image of cube shaped Au nanoparticles over 2D sheet. STEM-HAADF images (figure 5(c)) revealed brighter contrast for cube nanoparticles and relatively dull contrast for the 2D sheet. STEM-EDS compositional mapping revealed that the region of relatively dull contrast contained Cu and S atoms which in the light of the XRD results strongly indicate that the 2D sheet is Cu-thiolate. Results from the STEM-EDS compositional mapping experiment is shown in figure 5(d). Note that the XRD profile for the sample extracted after 5 minutes only showed diffraction peaks corresponding to pure Au and Cu-thiolate phases.

According to the XRD and TEM based analysis described above, it is suggested that during the initial stages of the synthesis reaction pure Au nanoparticles and 2D sheet Cu-thiolate complex are formed. Au nanocubes are adsorbed on the surface of the copper thiolate complex. With the progress of the synthesis process thermal decomposition of the thiolate complex occurs leading to the growth of copper (I) sulphide on the surface of Au-rich nanocube which is in

contact with the copper thiolate complex. A schematic illustrating the Au–Cu₂S hybrid nanostructure formation mechanism is shown in figure 6.

Effect of dodecanethiol (DDT) on morphology of hybrid nanoparticles

Effect of dodecanethiol (DDT) surfactant on the morphology of the hybrid nanoparticles was investigated by varying DDT amount from 0.3 mL, 1.0 mL and 3.0 mL in three different reaction mixtures containing 0.0339 g of HAuCl₄, 0.0455g of Cu(acac)₂, 1.6 g of HDD, 2.0 g of HDA, 0.270 g of ACA, and 10 mL of diphenyl ether. It has been shown in the literature that DDT can react with Cu(acac)₂ to produce Cu–dodecanethiol complex in the reaction mixture. This complex then undergoes cleavage of a C–S bond to produce a sulfur source that promotes the growth of Cu₂S nanocrystal³². Each reaction mixture was heated to ~180°C and was maintained at this temperature for 300 minutes. Following this, the solution was allowed to cool down to the room temperatures. At room temperature the reaction mixture was poured into a beaker containing ethanol. Nanoparticles isolated from reaction mixtures through high speed centrifugation were washed and re-dispersed in hexane for further study.

X-Ray diffraction profiles obtained from nanoparticles synthesized using various amounts of DDT are shown in figure 7(a). Two important observations that can be made from the XRD profiles are: (a) narrowing of the (111) peak of Au-rich phase with increase in the DDT amount. This is illustrated in the figure 7(b) which plots the variation of the Scherrer size of the Au-rich particles, which produces the (111) peak, with amount of DDT used in the reaction mixture and (b) appearance and increase in the intensity of the diffraction peaks corresponding to the Cu₂S phase with increasing in the DDT amount. TEM bright field image of the nanoparticles synthesized by using 0.3, 1.0 and 3.0 mL of DDT are shown respectively in figures 7(c-e). The

insets in figure 7 (c-e) shows the SAD pattern obtained from the nanoparticles seen in the TEM bright field images. Variation in the average size (as obtained from the summation average of sizes of several nanoparticles in the TEM bright field images) of the Au rich cube phase with the amount of DDT also plotted in figure 7(b) again reveals that size of the Au-rich cube phase increases with increase in the DDT amount. It can be seen that nanoparticles dispersion synthesized using 0.3 mL of DDT contain mostly cube shaped nanoparticles. The fraction of hybrid nanoparticles is extremely low. This result is in accordance with the corresponding XRD profile that revealed diffraction signature corresponding only to the fcc Au-rich phase. The nanoparticles synthesized using 1.0 mL of DDT contains uniform hybrid nanoparticles (the characterization study presented in the earlier parts of the paper investigates nanoparticles produced from using 1.0 mL of DDT). Nanoparticles synthesized using 3.0 mL of DDT contains spherical Cu_2S nanoparticles and larger sized Au-rich nanoparticles of different morphologies. These results clearly demonstrated that the concentration of DDT in the reaction mixture can be used to tune the microstructure and morphology of the Au- Cu_2S nanoparticles.

Conclusion

A modified polyol method for synthesizing uniform Au- Cu_2S hybrid nanoparticles is provided. Interest in Au- Cu_2S hybrid nanoparticles is due to the fact that in this system an interfacial electron transfer happens from the Cu_2S to the Au phase which enhances the oxidative degradation of dyes in the presence of these hybrid nanoparticles¹¹. As-synthesized hybrid nanoparticles contained cube shaped Au-rich, Au-Cu solid solution phase and hemispherical shaped Cu_2S phase. Mechanism of formation of hybrid nanoparticles involved initial formation of isolated Au nanoparticles with a cube morphology adsorbed over a Cu-thiolate complex with

an irregular 3D morphology. With increase in reaction time the Cu–thiolate complex decomposed to yield hemispherical Cu₂S phase formed over a Au-rich cube shaped phase. An optimum concentration of dodecanethiol is required both for achieving size and morphological uniformity of the participating phases and for their attachment to form a hybrid nanoparticle.

Acknowledgement

The authors acknowledge the electron microscopy facilities available at the Advanced Centre for microscopy and microanalysis (AFMM) Indian Institute of Science, Bangalore. One of the authors (S. K. Sinha) would acknowledge funding from the Council of Scientific and Industrial Research (CSIR), Government of India. C. Srivastava acknowledges the funding received from Nano-mission grant by Department of Science and Technology, Govt. of India.

References

- [1] R. Costi, A. E. Saunders and U. Banin, *Angew. Chem. Int. Ed.*, 2010, **49**, 4878-4897.
- [2] L. Carbone and P. D. Cazzoli, *Nano Today* 2010, **5**, 449-493.
- [3] W. Shi, H. Zeng, Y. Sahoo, T. Y. Ohulchanskyy, Y. Ding, Z. L. Wang, M. Swihart and P. N. Prasad, *Nano Lett.* 2006, **6**, 875-881.
- [4] P. D. Cozzoli, T. Pellegrino, L. Manna, *Chem. Soc. Rev.* 2006, **35**, 1195-1208.
- [5] J. Luo, L. Ma, T. He, C. F. Ng, S. Wang, H. Sun and H. J. Fan, *J. Phys. Chem. C* 2012, **116**, 11956-11963.
- [6] X. Xia, J. Tu, Y. Zhang, X. Wang, C. Gu, X. B. Zhao and H. J. Fan, *ACS Nano* 2012, **6**, 5531-5538.

- [7] R. Costi, A. E. Saundars, E. Elmalem, A. Salant, U. Banin, *Nano Lett.* 2006, **8**, 637-641.
- [8] E. Elmalem, A. E. Saundars, R. Costi, A. Salant and U. Banin, *Adv. Mater.* 2008, **20**, 4312-4317.
- [9] T. Yu, J. Zeng, B. Lim and Y. Xia, *Adv. Mater.* 2010, **22**, 5188-5192.
- [10] W. H. Hung, M. Aykol, D. Valley, W. Hou, *Nano Lett.* 2010, **10**, 1314-1318.
- [11] Y. Kim, K. Y. Park and D. M. Jang, Y. M. Song, H. S. Kim, Y. J. Cho, Y. Myung and J. Park, *J. Phys. Chem. C* 2010, **114**, 22141-22146.
- [12] C. Xu, J. Xie, D. Ho, C. Wang, N. Kohler, E. G. Walsh, J. R. Morgan, Y. E. Chin and S. Sun, *Angew. Chem. Int. Ed.* 2008, **47**, 173-176.
- [13] J. E. Macdonald, M. Bar Sadan, L. Houben, I. Popov, U. Banin, *Nature Mater.* 2010, **9**, 810-815.
- [14] T. Mokari, E. Rothenberg, I. Popov, R. Costi and U. Banin, *Science* 2004, **304**, 1787-1790.
- [15] A. Figuerola, A. Fiore, R. Di Corato, A. Falgui, C. Giannini, E. Micotti, A. Lascialfari, M. Corti, R. Cingolani, T. Pellegrino, P. D. Cozzoli, and L. Manna, *J. Am. Chem. Soc.* 2008, **130**, 1477-1487.
- [16] C. Wang, C. Xu, H. Zeng, and S. Sun, *Adv. Mater.* 2009, **21**, 3045-3052.
- [17] C. Wang, H. Dimon and S. Sun, *Nano Lett.* 2009, **9**, 1493-1496.
- [18] M. B. Cortie and A. M. McDonagh, *Chem. Rev.* 2011, **111**, 3713-3735.
- [19] M. R. Buck, J. F. Bondi and R. E. Schaak, *Nature Chem.* 2012, **4**, 37-44.
- [20] G. Krylova, L. J. Giovanetti, F. G. Requejo, N. M. Dimitrijevic, A. Prakapenka and E. V. Shevchenko, *J. Am. Chem. Soc.* 2012, **134**, 4384-4392.
- [21] D. Wang and Y. Li, *J. Am. Chem. Soc.* 2010, **132**, 6280-6281.

- [22] C. Wang, W. Tian, Y. Ding, Y. Q. Ma, Z. L. Wang, N. M. Markovic, V. R. Stamenkovic, H. Diamon, and S. Sun, *J. Am. Chem. Soc.* 2010, **132**, 6524-6529.
- [23] Y. Feng, J. He, H. Wang, Y. Y. Tay, H. Sun, L. Zhu, and H. Chen, *J. Am. Chem. Soc.* 2012, **134**, 2004-2007.
- [24] H. Gu, R. Zheng, X. Zhang and B. Xu, *J. Am. Chem. Soc.* 2004, **126**, 5664-5665.
- [25] L. L. Schramm, E. N. Stasiuk, and D. G. Marangoni, *Annu. Rep. Prog. Chem., Sect. C* 2003, **99**, 3-48
- [26] Y. Zhao and C. Burda, *Energy Environ. Sci.* 2012, **5**, 5564-5576.
- [27] Y. Wu, C. Wadia, W. Ma, B. Sadtler and A. P. Alivisatos, *Nano Lett.* 2008, **8**, 2551-2555.
- [28] S. Shen, Z. Tang, Q. Liu, and X. Wang, *Inorg. Chem.* 2010, **49**, 7799-7807.
- [29] N. E. Molt, J. F. Bondi and R. E. Schaak, *Chem. Mater.* 2012, **24**, 1552-1554.
- [30] X. Ding, Y. Zou and J. Jiang, *J. Mater. Chem.* 2012, **22**, 23169-23174.
- [31] Y. Liu and A. R. Hight Walker, *Angew. Chem. Int. Ed.* 2010, **49**, 6781-6785.
- [32] A. Tang, S. Qu, K. Li, Y. Hou, F. Teng, J. Cao, Y. Wang, and Z. Wang, *Nanotechnology* 2010, **21**, 285602-1-285602-9.
- [33] B. D. Cullity and S. R. Stock, *Element of X-Ray Diffraction. Third Edition, Prentice Hall Publishing Inc.* 2001, 339.
- [34] H. Okamoto, D. J. Chakrabarti, D. E. Laughlin and T. B. Massalski, *Bulletin of Alloy Phase Diagrams* 1987, **8**, 454-473.
- [35] S. Khanal, G. Casillas, N. Bhattarai, J. J. Velázquez-Salazar, U. Saniago, A. Ponce, S. Mejía-Rosales, M. José-Yacamán, *Langmuir* 2013, **29**, 9231-9239.

Figure captions

Figure 1. (a) TEM bright field image, (b) STEM-HAADF image of as synthesized Au–Cu₂S hybrid nanostructures, (c) reconstructed images obtained from three-dimensional tomographic imaging of a representative hybrid nanoparticle in TEM, (d) X-Ray diffraction, and (e) selected area diffraction (SAD) patterns obtained from as synthesized Au–Cu₂S hybrid nanostructures. The insert in figure 1(d) shows the XRD profile in the 2 Θ range of 45-70° containing diffraction peaks corresponding to the Cu₂S phase.

Figure 2. (a) STEM-HAADF image of hybrid nanoparticles and composition values obtained at point '1' and '2' (b) STEM-EDS composition mapping result showing STEM-HAADF image (b1), Au rich region (b2), Cu rich region (b3) and S rich region (b4).

Figure 3. (a) High-resolution TEM image of Au rich nanocube part of a representative hybrid nanoparticle. Inset shows FFT pattern obtained from the ROI denoted by the square, magnified image of the ROI and the reconstruction lattice, (b) High-resolution TEM image of hemispherical Cu₂S phase part of a hybrid nanoparticle. Inset shows FFT pattern obtained from the ROI denoted by square, magnified image of ROI and reconstruction lattice, (c) High-resolution TEM image of a hybrid nanoparticle showing 3 different ROIs denoted by squares. The upper left FFT is obtained from ROI 1 and lower right FFT is obtained from ROI 3. The upper right FFT is from the cube-hemisphere interface (ROI 2). The right most figure shows the magnified view of the interface and the corresponding reconstruction lattice illustrating the orientation relationship: [001] Au//[0001] Cu₂S and (200) Au//(1100)Cu₂S. Lattice models and reconstruction lattice were obtained using Diamond 3.2 software.

Figure 4. X-Ray diffraction profile of specimens extracted at 180°C temperature after 5, 180, and 300 minutes. Fig 4(a) contains XRD profiles for the full 2-theta range from 10 to 90; Fig

4(b) contains XRD profiles for the 2-theta range of 10 to 35; Fig 4(c) contains XRD profiles for the 2-theta range of 35 to 50; Fig 4(d) Contains XRD profiles for the 2-theta range of 50 to 90.

Figure 5. (a) TEM bright field image of cube shape Au nanoparticle. Inset shows selected area diffraction pattern from cube shaped nanoparticles, (b) Low magnification TEM bright-field image showing Cu-thiolate complex along with Au nanoparticles, (c) STEM-HAADF image of Cu-thiolate complex along with Au nanoparticles, (d) STEM-EDS composition mapping result of intermediate complex attached to Au-cube, showing Au, Cu and S containing regions.

Figure 6. Schematic illustration of the formation mechanism of $\text{Au}_{1-x}\text{Cu}_x\text{-Cu}_2\text{S}$ hybrid nanoparticles.

Figure 7. (a) X-Ray diffraction pattern of nanoparticles prepared from reaction mixture containing different amount of dodecanethiol (DDT), (b) variation in the average size of the Au rich region with change in the amount of DDT. TEM bright field image of nanoparticles obtained from the reaction mixture containing (c) 0.3 mL, (d) 1.0 mL, and (e) 3.0 mL of dodecanethiol amount. Inset shows the SAD pattern obtained from nanoparticles.

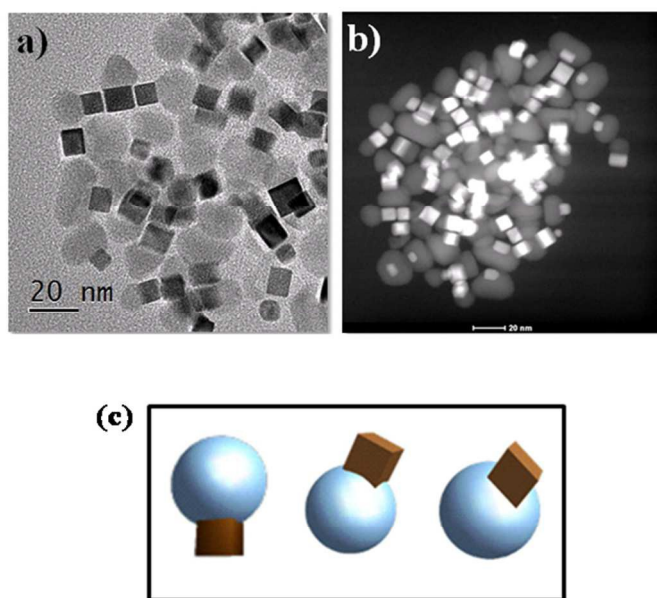
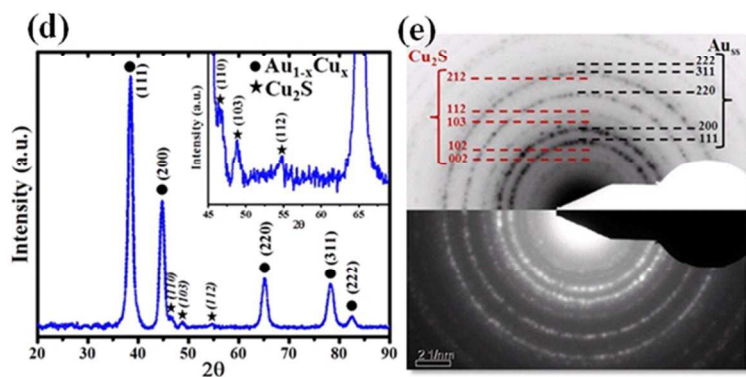


Figure 1

254x190mm (96 x 96 DPI)

**Figure 1**

254x190mm (96 x 96 DPI)

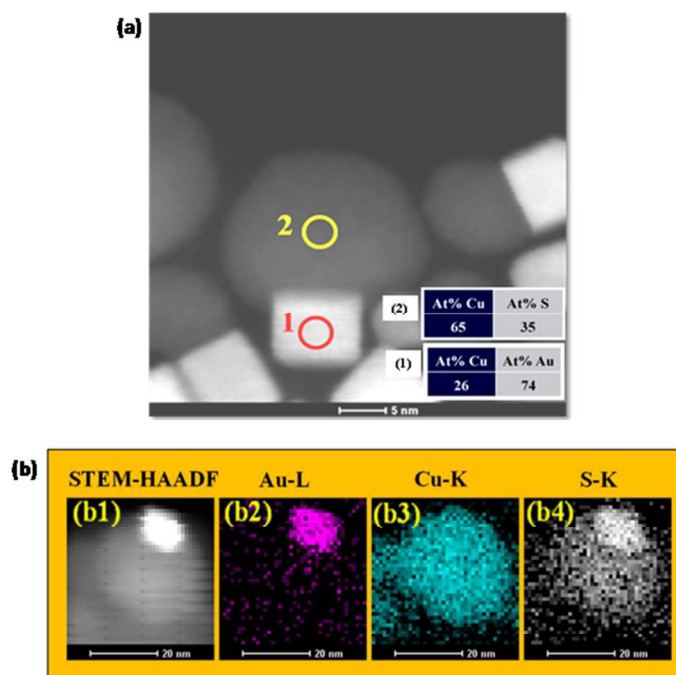
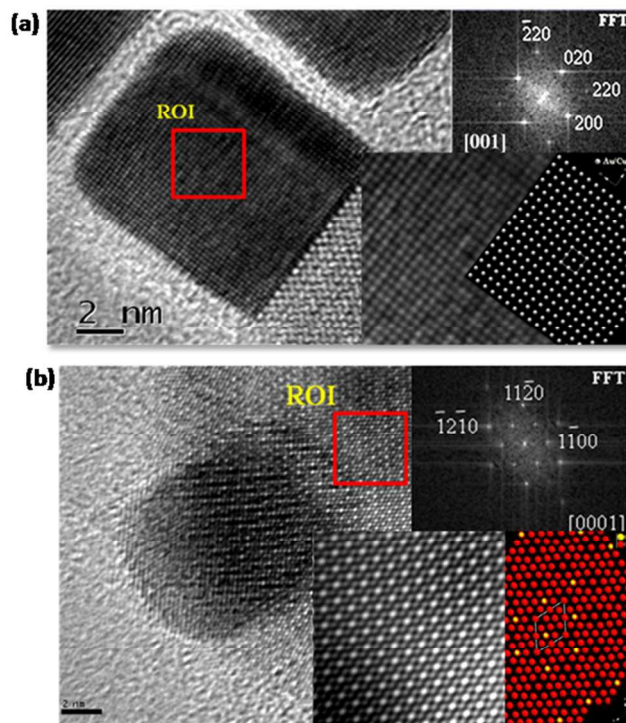


Figure 2

254x190mm (96 x 96 DPI)

**Figure 3**

254x190mm (96 x 96 DPI)

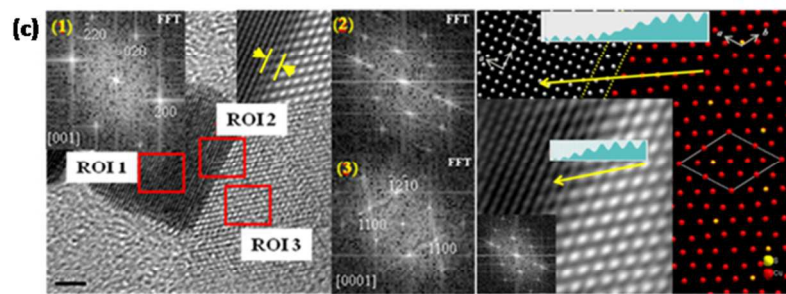
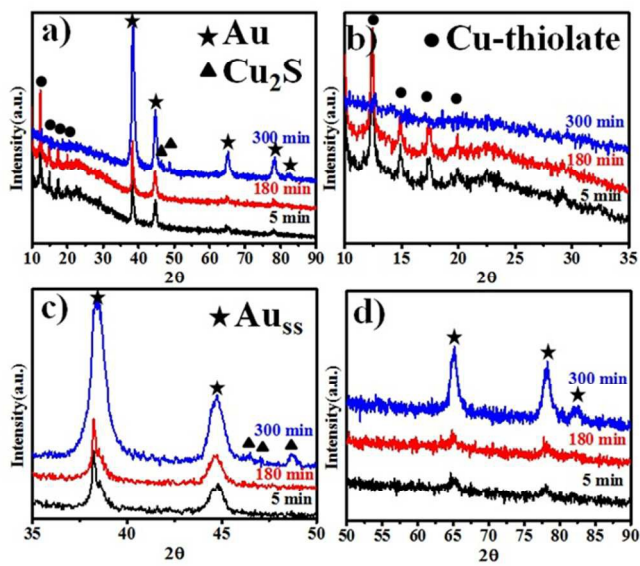
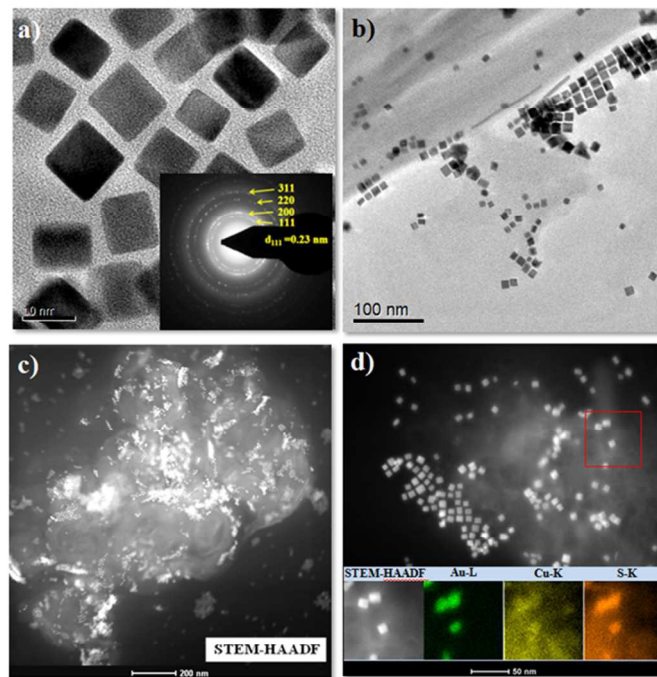


Figure 3

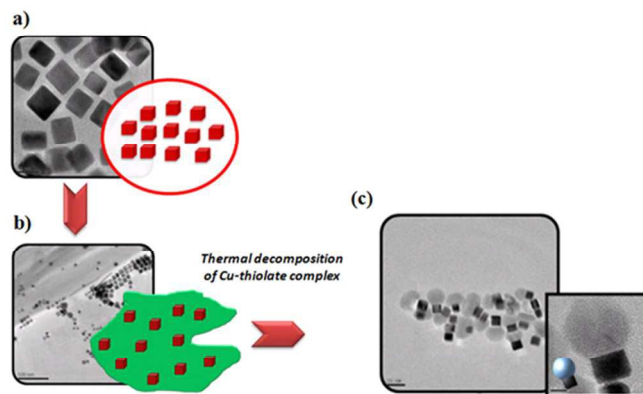
254x190mm (96 x 96 DPI)

**Figure 4**

254x190mm (96 x 96 DPI)

**Figure 5**

254x190mm (96 x 96 DPI)

**Figure 6**

254x190mm (96 x 96 DPI)

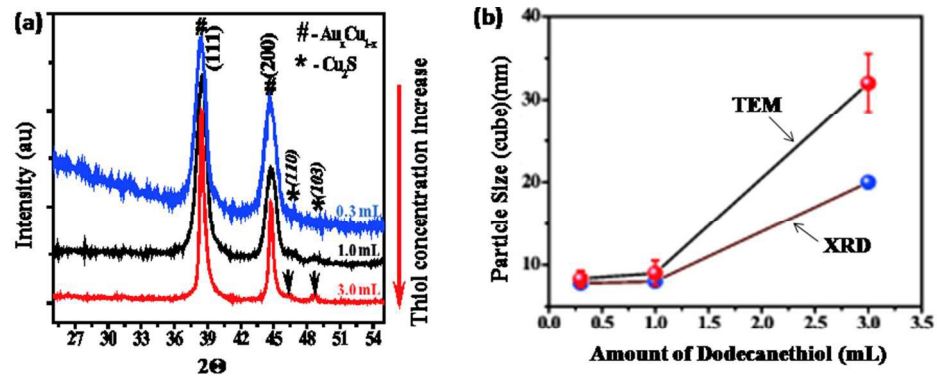


Figure 7

254x190mm (96 x 96 DPI)

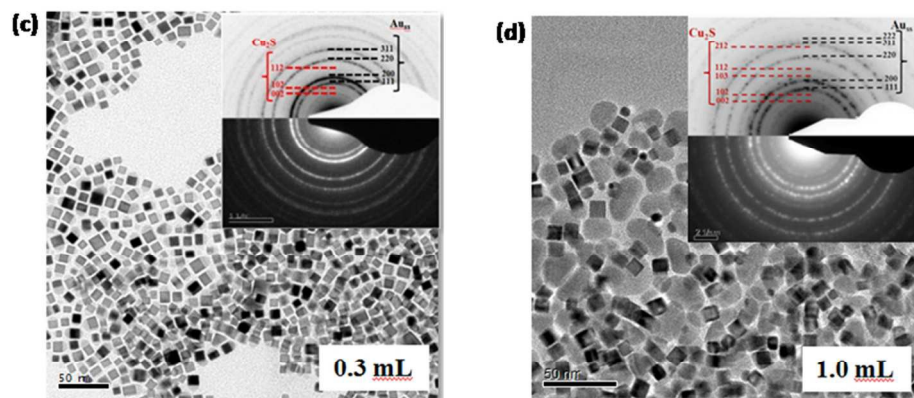


Figure 7

254x190mm (96 x 96 DPI)

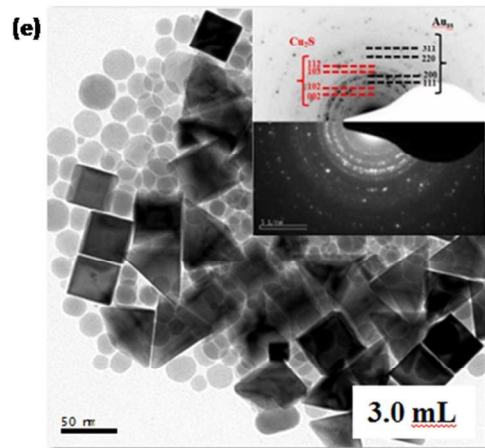


Figure 7

254x190mm (96 x 96 DPI)